Journal of ELECTRICAL ENGINEERING, VOL. 55, NO. 11-12, 2004, 290–295

CONTOUR IMAGE DATA COMPRESSION USING SPLINE WAVELETS

Zoltán Szabó *

The presented paper is motivated by seeking an efficient encoding scheme for arbitrarily shaped objects using linear, quadratic and cubic spline wavelets. A new contour image data compression method is described and its efficiency evaluated from the achieved bit-per-contour-pixel ratio point of view.

K e y w o r d s: wavelet transform, spline wavelets, contour coding

1 INTRODUCTION

There are many applications where the shape of objects needs to be encoded, such as CAD, 3D modelling, signature encoding [9], as well as region oriented video coding techniques [1], where the shape information is described by a binary mask having the same values for all the pixels inside the shape. The binary mask indicates the region(s) in which the texture of the object needs to be coded [7]. Contours around the shape in binary masks are generally simple closed ones, without intersection and ambiguous contour continuations (see Figure 1). They are defined usually in pixel resolution, consisting of a number of adjacent pixels that are called contour points. They can be represented, *eg*, by a chain code [8] or approximated with a polynomial function and subsequently entropy coded [9]. In our case the contour image is converted to its parametric representation and coded with spline wavelets.

1.1 Brief introduction to wavelet theory

The wavelet transform (WT) of a real function $s(t)$ is defined as [1]:

$$S(\lambda,\tau)=\frac{1}{\sqrt{\lambda}}\int_{-\infty}^{\infty}s(t)\psi\left(\frac{t-\tau}{\lambda}\right)\mathrm{d}t \qquad (1)$$

where $\psi(t)$ is a zero mean mother wavelet. The final function $S(\lambda,\tau)$ as well as the particular wavelets are described with two parameters: time shift τ also called translation factor and dilation parameter λ, known as the scale factor. The normalisation constant $\lambda^{-1/2}$ compensates the different energies of wavelets.

The special case of wavelet transform described above is a dyadic discrete wavelet transform (DWT), where the dilation parameter $\lambda=2^m$, and the translation factor $\tau=2^m k$, $m>0$, k and m are integer numbers. The dyadic DWT can be realised with the bank of filters having impulse responses h_m [1].

For discrete signal $s(n)$, the dyadic wavelet transform (DTWT) is defined:

$$S_m(k)=\sum_{n=-\infty}^{\infty}s(n)h_m\left(2^m k-n\right). \qquad (2)$$

The wavelet decomposition realised with the bank of filters broke down a signal into many lower-resolution components (frequency bands) by low-pass end high-pass filters (see Fig. 2).

Generally the output from any low-pass filter can be split iteratively until the last branch consists of a single sample. In practice, the suitable number of levels is based on the nature of the signal, or on the application [9].

The wavelet reconstruction filter-banks structure is similar to the decomposition structure:

The conditions for perfect reconstruction $s(n)=s'(n)$, are given by the following formulae [1]:

$$\begin{aligned}F_{LP}(z)H_{LP}(z)+F_{HP}(z)H_{HP}(z)&=2\,,\\ F_{LP}(z)H_{LP}(-z)+F_{HP}(z)H_{HP}(-z)&=0\,.\end{aligned} \qquad (3)$$

Note: The conditions above and block diagram in Fig. 3 are valid, when non-causal filter-banks are considered with zero time delay. Otherwise time delay blocks should be entered into particular branches.

Several different approaches exist for filter-banks design that create orthogonal or biorthogonal structures [8]. The structure of the orthogonal filter-banks is very special. For example, if the length of their impulse response is four: all filters (decomposition HP, LP and reconstruction HP, LP filters) use four coefficients a, b, c, d, where the convolution along the bottom channel (multiplication of polynomials $H_{LP}(z)=a+bz^{-1}+cz^{-2}+dz^{-3}$ and $F_{LP}(z)=d+cz^{-1}+bz^{-2}+az^{-3}$ — see Fig. 4) gives a particular "halfband filter" [8]. For this example the halfband filter coefficients are $(-1/16,\ 0,\ 9/16,\ 1,\ 9/16,\ 0,\ -1/16)$. Note: The odd powers of z^{-1} are missing for this type of filter.

* Institute for Biomedical Engineering, Czech Technical University in Prague, nam. Sitna 3105, 272 01 Kladno 2, Czech Republic, e-mail: szabo@ubmi.cvut.cz

ISSN 1335-3632

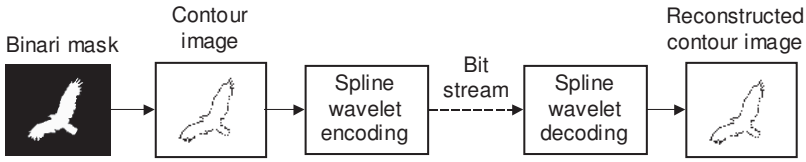

Fig. 1. The scope of contour image coding.

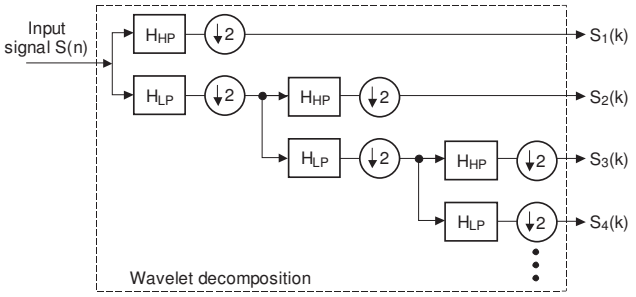

Fig. 2. Dyadic wavelet transform realised with the tree structure of high-pass (H_{HP})and low-pass (H_{LP}) decomposition filters. Note: The circles represent down-sampling with a factor of two (the odd numbered components are removed after filtering).

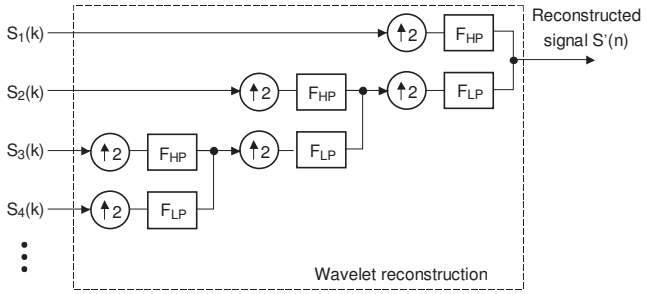

Fig. 3. Inverse dyadic wavelet transform realised with the tree structure of high-pass (F_{HP}) and low-pass (F_{LP}) reconstruction filters. Note: The up-sampling operation $\uparrow 2$ inserts zeros between the samples.

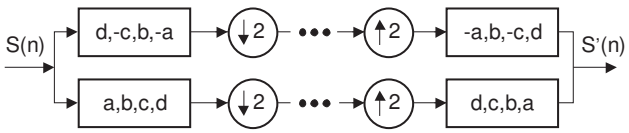

Fig. 4. The form of the orthogonal filter bank with four coefficients. The left part corresponds with the decomposition (analysis) and the right part corresponds with the reconstruction (synthesis) part of the wavelet transform.

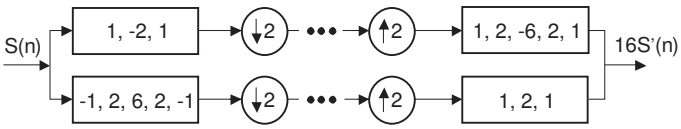

Fig. 5. The biorthogonal filter bank

The biorthogonal filter-bank design is less restricted than the design of an orthogonal one. The multiplication of two polynomials along the bottom channel gives also the halfband filter, but the reconstruction low-pass filter coefficients do not have to be the transpose (the flip) of the decomposition low-pass filter coefficients. Figure 5 shows how the filters on the reconstruction side are related to the decomposition filters. The relation between their transfer functions is derived from the equation 3 giving the following formulas:

$$F_{LP}(z) = H_{HP}(-z)\,, \quad F_{HP}(z) = -H_{LP}(-z)\,, \qquad (4)$$

where the simple substitution $z \to -z$ provides a high-pass filter based on the low-pass one, or vice versa [10]. In time-domain it corresponds with multiplying the elements of $h(k)$ with $(-1)^j$, $j = 0, 1, \ldots$.

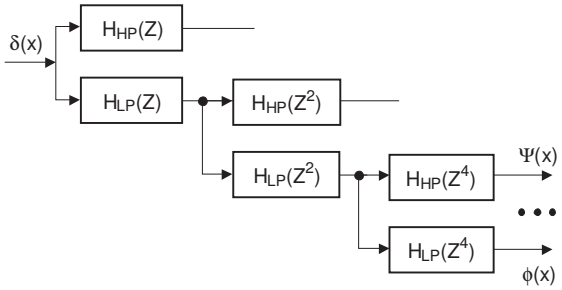

Fig. 6. Scaling function $\phi(x)$ and wavelets $\psi(x)$ from iteration of the low-pass filters. Where: $\delta(x)$ is the Dirac delta function, $H_{HP}(z)$ is a transfer function of the highpass filter, $H_{HP}(z^2)$ is a modified transfer function of the highpass filter (the filter coefficients are zero padded).

The above-mentioned discrete-time filters have the following relation with the continuous-time wavelets $\psi(t)$. The approximation of wavelets (their shape) comes from the iterative convolution of impulse responses of the rescaled filters as it is shown in Fig. 6. Continuing the decomposition we approximate more and more the

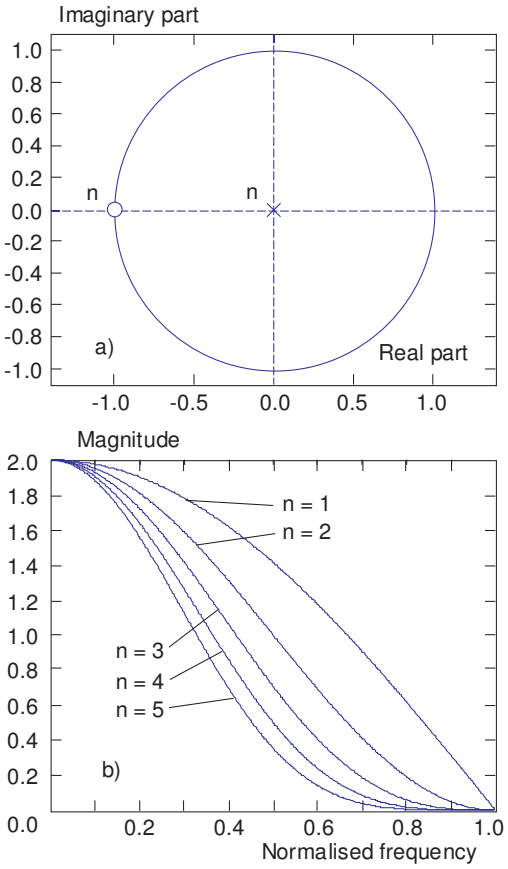

Fig. 7. The representation of low-pass filters $F_{LP}(z)$ in z-plane (a). Their frequency responses for five different values of n (b). Note: Normalised frequency=1 corresponds to half the sample rate.

continuous-time wavelets' shape [8]. The output from the last LP filter approximates the so-called scaling function $\phi(t)$ and the output from the last HP filter approximates the continuous-time wavelet $\psi(t)$.

2 SPLINE WAVELET TRANSFORM

We have a spline wavelet transform whenever the synthesis functions ($\psi(t)$ and $\phi(t)$) are polynomial splines of degree n [10]. It can be proved that using low-pass filter with coefficients $(1,1)$ and derivation of the scaling function according to the Figure 6 we will get the first order B-spline basis function $B_{0,1}(t)$ [9]. Filter coefficients $(1/2,1,1/2)$ lead to the linear spline basis function $B_{0,2}(t)$, filter coefficients $(1/4,3/4,3/4,1/4)$ lead to the quadratic spline basis function $B_{0,3}(t)$, and filter coefficients $(1/8,1/2,3/4,1/2,1/8)$ lead to the cubic spline basis function $B_{0,4}(t)$.

The same filter coefficients can be derived by repeated convolutions of the coefficients $h^1=(1,1)$ as follows:

$$h^n(k)=\frac{1}{2^{n-1}}h^1(k)*h^1(k)*\cdots*h^1(k) \qquad (5)$$

where n is the number of repetition of $h^1(k)$ in the equation. The low-pass filter coefficient associated with the nth order B-spline can be simply generated also by binomial series development [8]:

$$h^n(k)=\frac{1}{2^n}\frac{(n+1)!}{(n+1-k)!k!},k=0,1,\ldots,n+1 \qquad (6)$$

The z transform of the sequence of filter coefficients $h^n(k)$ is the following:

$$F_{LP}(z)=\frac{1}{2^{n-1}}\left(1+z^{-1}\right)^n=2\left(\frac{1+z^{-1}}{2}\right)^n=2\left(\frac{z+1}{2z}\right)^n. \qquad (7)$$

The configuration of zeros and poles are illustrated in Fig. 7a, where zeros of multiplicity n are placed on the real axes at point -1, and poles of multiplicity n are in the centre of z-plane. The frequency responses for five different n are shown in Fig. 7b. Note: $n=3$ corresponds to the quadratic- and $n=4$ corresponds to the cubic-spline scaling function $\phi(t)$. Hereafter, the other filter coefficients are derived.

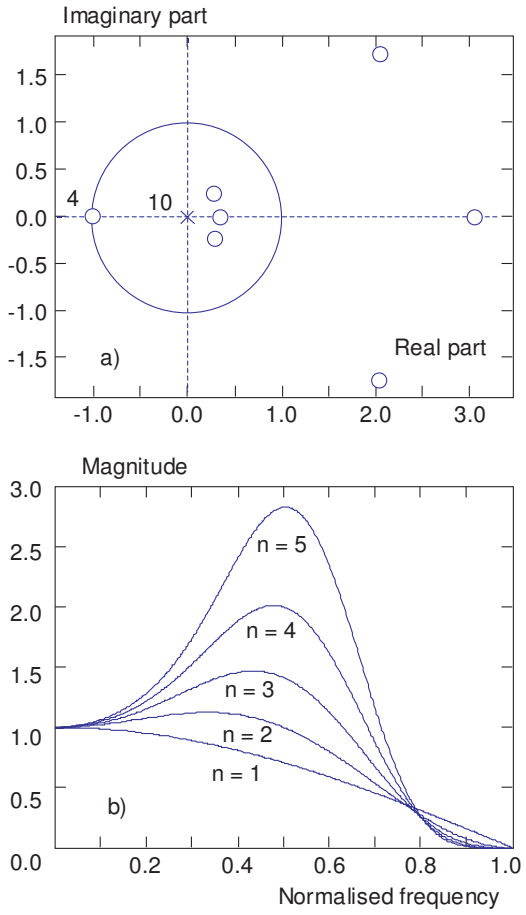

Fig. 8. The representation of decomposition low-pass filters $H_{LP}(z)$ in z-plane for $n=4$ (a). The frequency responses for five different values of n (b). Note: Normalised frequency=1 corresponds to half the sample rate.

Table 1. Low-pass filter coefficients for biorthogonal wavelet decomposition and reconstruction. $h^n(k)_{\mathrm{DEC}}$ stands for decomposition- and $h^n(k)_{\mathrm{REC}}$ stands for reconstruction-filter coefficients.

LP filters		Low-pass filter coefficients
$n=1$	$h^1(k)_{\mathrm{DEC}}$	1/2, 1/2
	$h^1(k)_{\mathrm{REC}}$	1, 1
$n=2$	$h^2(k)_{\mathrm{DEC}}$	-1/8, 1/4, 3/4, 1/4, -1/8
	$h^2(k)_{\mathrm{REC}}$	1/2, 1, 1/2
$n=3$	$h^3(k)_{\mathrm{DEC}}$	3/64, -9/64, -7/64, 45/64, 45/64, -7/64, -9/64, 3/64
	$h^3(k)_{\mathrm{REC}}$	1/4, 3/4, 3/4, 1/4
$n=4$	$h^4(k)_{\mathrm{DEC}}$	-0.0195, 0.0781, -0.0039, -3/8, 0.2734, 1.0938, 0.2734, 3/8, 0.0039, 0.0781, -0.0195
	$h^4(k)_{\mathrm{REC}}$	1/8, 1/2, 3/4, 1/2, 1/8

Table 2. High-pass filter coefficients for biorthogonal wavelet decomposition and reconstruction. $g^n(k)_{\mathrm{DEC}}$ stands for decomposition- and $g^n(k)_{\mathrm{REC}}$ stands for reconstruction-filter coefficients.

HP filters		High-pass filter coefficients
$n=1$	$g^1(k)_{\mathrm{DEC}}$	1, -1
	$g^1(k)_{\mathrm{REC}}$	-1/2, 1/2
$n=2$	$g^2(k)_{\mathrm{DEC}}$	1/2, -1, 1/2
	$g^2(k)_{\mathrm{REC}}$	1/8, 1/4, -3/4, 1/4, 1/8
$n=3$	$g^3(k)_{\mathrm{DEC}}$	1/4, -3/4, 3/4, -1/4
	$g^3(k)_{\mathrm{REC}}$	-3/64, -9/64, 7/64, 45/64, -45/64, -7/64, 9/64, 3/64
$n=4$	$g^4(k)_{\mathrm{DEC}}$	1/8, -1/2, 3/4, -1/2, 1/8
	$g^4(k)_{\mathrm{REC}}$	0.0195, 0.0781, 0.0039, -3/8, -0.2734, 1.0938, -0.2734, -3/8, 0.0039, 0.0781, 0.0195

As it was mentioned before the multiplication of two polynomials (in z-plane: the multiplication of transfer functions $H_{LP}(z)$ and $F_{LP}(z)$) along the bottom channel (Figures 4 and 5) gives the so-called half band filter [8]. Therefore, if one of these polynomials will compose the spline scaling function, then the second one can be derived from the half band filter transfer function [8]:

$$P(z) = 2\Big(\frac{1+z^{-1}}{2}\Big)^n \Big(\frac{1+z}{2}\Big)^n \sum_{i=0}^{n-1} \binom{n+i-1}{i} \times \Big(\frac{1-z}{2}\Big)^i \Big(\frac{1-z^{-1}}{2}\Big)^i = F_{LP}(z) H_{LP}(z)\,. \quad (8)$$

The first part of the expression above represents the reconstruction low-pass filter leading to the spline scaling function (see Equation 7) and the second part represents the transfer function of the decomposition low-pass filter $H_{LP}(z)$. The configuration of zeros and poles for $n = 4$ is illustrated in Fig. 8a. The frequency responses for $n = 1, 2, \ldots, 5$ are shown in Fig. 8b.

The filter coefficients of decomposition and reconstruction part for $n = 1, 2, 3, 4$ are summarised in Tables 1 and 2.

3 CONTOUR IMAGE DATA COMPRESSION USING SPLINE WAVELETS

Wavelet transform offers good properties for data compression. The signal-decomposition to several frequency bands leads even to the signals with low entropy and thereby to more efficient entropy coding. The process of contour image compression/decompression with wavelet transform is shown in Fig. 9.

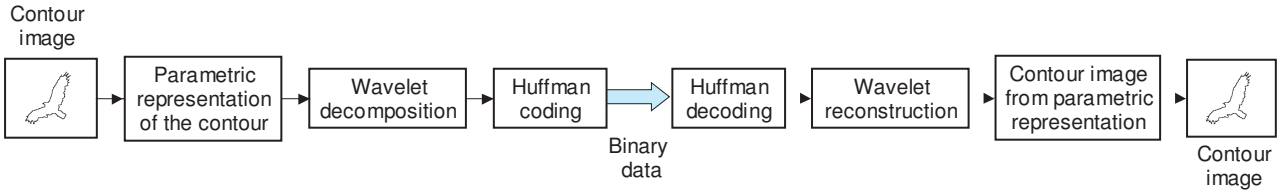

Fig. 9. Wavelet-based contour image coding and reconstruction.

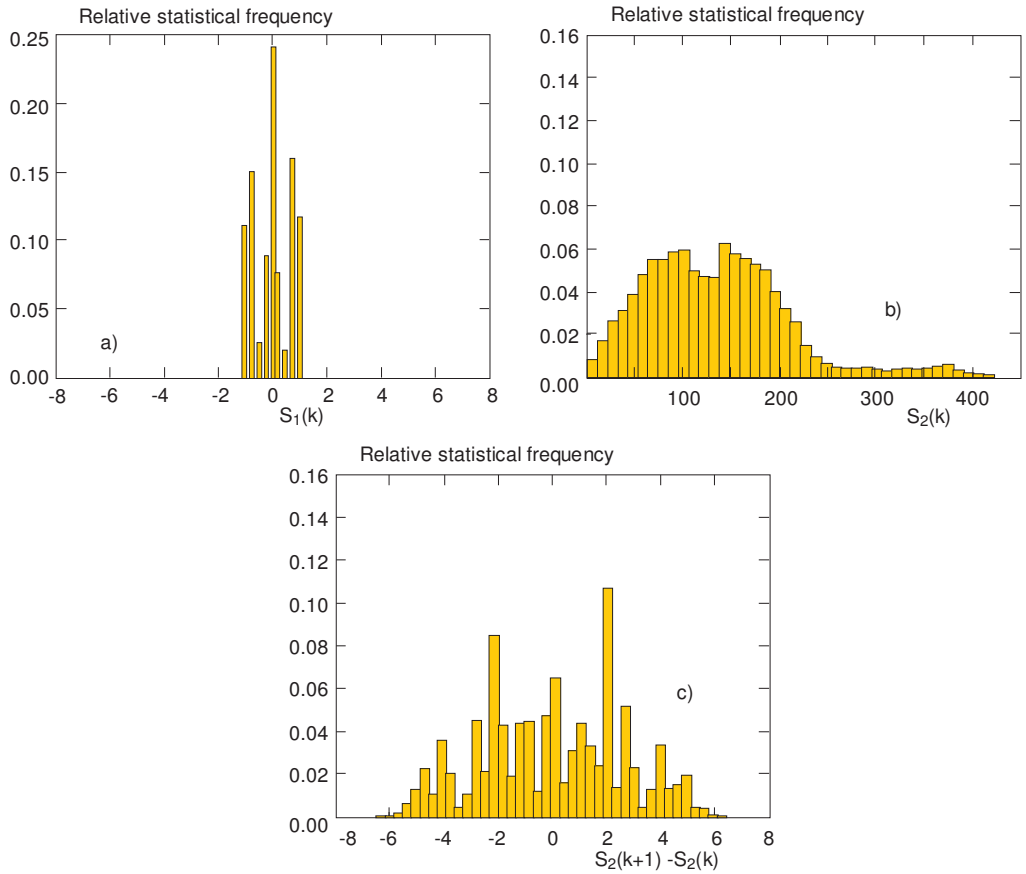

Fig. 10. Relative statistical frequencies of the $S_1(k)$ — output from the HP decomposition filter (a), $S_2(k)$ — output from the LP decomposition filter (b), $S_2(k+1) - S_2(k)$ — differences of the successive samples of the output from the HP decomposition filter (c).

The two-dimensional discrete contour is represented as a set of two discrete parametric functions $x(k)$ and $y(k)$, where parameter k indicates the pixel position at the contour. These functions are decomposed by wavelet transform (low-pass and high-pass filters) to frequency bands $S_m(k)$ and entropy coded with Huffman coding. The decompression is an inverse process, where the decoded binary data are transformed to parametric functions with wavelet reconstruction and displayed as the contour image.

The biorthogonal wavelet transform based on the filters listed in Tabs. 1 and 2 are reversible. It means, that perfect reconstruction is possible if the output from wavelet-decomposition-block $S_m(k)$ are with no change transformed back by reconstruction block. Higher data reduction can be achieved when $S_m(k)$ are thresholded (values not exceeding the threshold are set to zero) [1].

4 TEST RESULTS AND DISCUSSION

In our experiments, one level decomposition and reconstruction was used (Fig. 5) with three different types of filters ($n = 2$, $n = 3$, $n = 4$ — see Tabs. 1 and 2). The outputs from HP and LP filters ($S_1(k)$ and $S_2(k)$) were Huffman coded separately with different code tables derived from the image test set containing 60 contour images [9]. The output from the LP filter ($S_2(k)$) was differentially encoded instead of the direct Huffman coding, since the standard deviation is essentially reduced after differentiating (see Tab. 3). The relative statistical frequencies of the coded data are shown in Fig. 10.

Table 3. Statistical analysis of wavelet transformed contour image data. Note: These results are obtained with wavelet transform using LP reconstruction filter corresponding to the cubic B-spline scaling function ($n = 4$).

	$S_1(k)$	$S_2(k)$	$S_2(k+1) - S_2(k)$
Minimum	−1.47	5.97	−6.34
Maximum	1.17	417.13	6.24
Mean	0	134.39	0
Standard Deviation	0.65	73.68	2.62
Variance	0.43	5428.60	6.88

Table 4. The average bit-per-contour-pixel (bpcp) ratio for wavelet-based contour image compression.

(bpcp)	Wavelet type		
	$n = 2$ (linear)	$n = 3$ (quadratic)	$n = 4$ (cubic)
Huffman coded $S_1(k)$ and $S_2(k)$	4.71	2.65	1.52
Huffman coded $S_1(k)$ and $S_2(k+1) - S_2(k)$	0.53	1.02	0.29

5 CONCLUSION

The test results are summarised in Tab. 4. Two different approaches are compared: first, when the outputs from wavelet decomposition $S_1(k)$ and $S_2(k)$ are coded directly and second, when $S_2(k)$ is coded differentially. Three types of filters were used, presented in Tabs. 1 and 2, where $n = 2$ corresponds to linear-, $n = 3$ corresponds to quadratic-, and $n = 4$ corresponds to cubic-spline scaling function.

The transformed data $S_1(k)$ and $S_2(k)$ (as well as their differences) are real numbers, thanks to the fact that filter coefficients and the input signal are real. The Huffman coding requires their rounding to finite precision numbers, which causes that the reconstruction becomes lossy. Rounding the data before Huffman coding to one decimal precision causes an error between the original and the reconstructed signal approximately 0.17 units (in our case one unit is the distance between two successive pixels). This approximation error can be considered as almost negligible, as the next image processing point of view.

Comparing the results in Tab. 4 we can draw the following conclusions: a) The differentially encoded data of wavelet transform brings an essential improvement over their direct coding. Depending on the wavelet transform it is over 60 %. b) From the three tested wavelet types ($n = 2$, $n = 3$, $n = 4$), the third one ($n = 4$) is the most effective.

Note: The theory of wavelet compression offers more possibilities to explore and improve these results. Different types of wavelets can be used, the depth of tree decomposition can be changed or higher compression can be achieved with thresholding the wavelet-transformed data. Nevertheless, this would go beyond the frame of this paper.

Acknowledgements

This work has been supported by the grant No. CEZ J22/98:262200011 of the Research Programme of the Brno University of Technology. The author also wishes to thank the IMEC Research Centre in Leuven, Belgium for their technical support.

References

[1] BORMANS, J.: VLSI Implementation of Region Oriented Image Compression Algorithms, PhD Dissertation, Vrije Universiteit Brussel, April, 1998.

[2] EDEN, M.—KOCHER, M.: On the Performance of a Contour Coding Algorithm in the Context of Image Coding, Part I: Contour segment Coding, Signal Processing No. 8 (1985), 381–386.

[3] GONZALEZ, R. C.—WINTZ, P.: Digital Image Processing (Chapter 7 — Image segmentation), Addison-Wesley Publishing Company, 1987, pp. 331–389.

[4] GOSWAMI, J. C.—CHAN, A. K.: Fundamentals of Wavelets, Theory, Algorithms, and Applications, John Wiley & Sons, Inc., 1999.

[5] JAN, J.: Digital Signal Filtering, Analysis and Restoration, The Institution of Electrical Engineers, London, United Kingdom, IEE Telecommunications series 44, 2000.

[6] MISITI, M.—MISITI, Y.—OPPENHEIM, G.—POGGI, J.-M.: MATLAB Wavelet Toolbox Users Guide. March 1996.

[7] MITCHEL, J. S.—PENNEBAKER, W. B.—FOGG, C. E.—LeeGALL, D. J.: MPEG Video Compression Standard, Chapman & Hall, 1996.

[8] STRANG, G.—NGUYEN, T.: Wavelets and Filter Banks, Wellesley-Cambridge Press, 1996.

[9] SZABÓ, Z.: Contour Coding for Compression of Still Images and Image Sequences, Doctoral theses, Department of Biomedical Engineering, Brno University of Technology. 2001.

[10] UNSER, M.: Ten Good Reasons for Using Spline Wavelets, Proc. SPIE Vol. 3169, Wavelets Applications in Signal and Image Processing V (1997), 422–431.

Received 27 May 2004

Zoltán Szabó was born in Košice (former Czechoslovakia, now the Slovak Republic) in 1971. He received his Ing (MSc) degree in radioelectronics from the Technical University Košice in 1994 and PhD degree from the Brno University of Technology, Czech Republic in 2001. Since 2004 he has worked in the Institute for Biomedical Engineering, Czech Technical University in Prague as an assistant professor. His research interests include digital signal and image processing — image segmentation, motion detection, pattern recognition, machine vision, signal analysis and compression, medical electronic equipment.